THE JOURNAL OF PHYSICAL CHEMISTRY B

Article

pubs.acs.org/JPCB

NMR Study of Cation Dynamics in Three Crystalline States of 1-Butyl-3-methylimidazolium Hexafluorophosphate Exhibiting Crystal Polymorphism

Takatsugu Endo,[†] Hiroki Murata,[†] Mamoru Imanari,[‡] Noriko Mizushima,[§] Hiroko Seki,[‡] and Keiko Nishikawa*,[†]

[†]Graduate School of Advanced Integration Science, Chiba University, 1-33 Yayoi-cho, Inage-ku, Chiba 263-8522, Japan

[‡]Chemical Analysis Center, Chiba University, Yayoi, Inage-ku, Chiba 263-8522, Japan

[§]Laboratory of Clinical Pharmacy, Yokohama College of Pharmacy, Matano-cho 601, Totsuka, Yokohama 245-0066, Japan

ABSTRACT: We investigate the cation rotational dynamics of a room temperature ionic liquid (RTIL) 1-butyl-3-methylimidazolium hexafluorophosphate ([C_4mim]PF_6) in its three crystalline states by ^{1}H NMR spectroscopy. Spin−lattice and spin−spin relaxation time (T_1 and T_2, respectively) measurements as a function of temperature confirm the presence of three polymorphic crystals of [C_4mim]PF_6: crystals α, β, and γ, which we previously discovered using Raman spectroscopy and calorimetry. Second moment calculations of ^{1}H NMR spectra reveal that certain segmental motions of the butyl group in addition to the rapid rotation of the two methyl groups in the cation occur in all the crystals. The trend in the mobility of the segmental motions is $\gamma < \beta \leq \alpha$, which is consistent with the strength of cation−anion interactions (or crystal packing density) estimated from high-frequency Raman scattering experiments. T_1 measurements demonstrate two types of rotational motions on the nanosecond time scale in all three crystals: fast and slow motions. The three crystals have similar activation energies of 12.5−15.1 kJ mol^{-1} for the fast motion, which is assigned to the rotation of the methyl group at the terminal of the butyl group. These observed activation energies were consistent with that estimated by quantum chemical calculations in the gas phase (11.9 kJ mol^{-1}). In contrast, the slow motions of crystals α and γ are attributed to different segmental motions of the butyl group and that of crystal β to either a little segmental motion or a certain PF_6^- rotational motion. These nanosecond rotational motions obtained from the T_1 measurements do not appear to be affected by crystal packing density because local interactions in the crystalline state rather than packing density govern such nanosecond motions. With respect to the segmental motions, the mobility is likely to change significantly with the conformation of the butyl group. On the basis of these findings, crystal γ, which is the only crystalline phase previously determined using single-crystal X-ray diffraction, is considered to be the most stable phase because of the slowest segmental motions and the strongest cation−anion interactions.

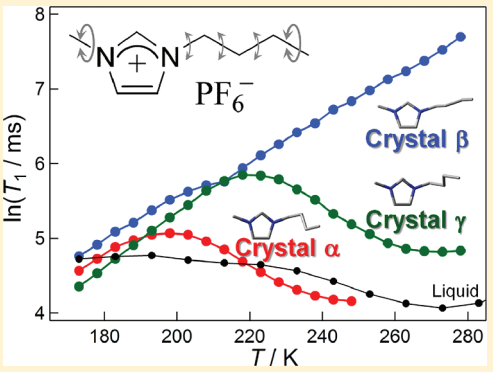

INTRODUCTION

Room temperature ionic liquids (RTILs) are salts that are liquids at or near room temperature. Because RTILs have several outstanding properties as liquids, such as negligible vapor pressure, extremely low flammability, unique solubility, and so forth, they are considered to be potentially useful as electrolytes in batteries and green solvents for organic syntheses among other applications.[1−5]

1-Butyl-3-methylimidazolium hexafluorophosphate ([C_4mim]PF_6, the chemical structure is shown in Figure 1) is known as a representative RTIL. Various physical properties of [C_4mim]PF_6 have been reported, e.g., melting point,[6−9] viscosity,[7,10−15] and density.[6−8,10−15] In addition, the molecular structure[16−25] and dynamics[16−18,22,23,26−31] in the liquid state have been reported by many researchers. On the other hand, the thermal phase behavior in the solid state, which is an important property of RTILs, is complicated and not completely understood.[8,32,33] Our group recently revealed that [C_4mim]PF_6 has three crystalline phases with different butyl conformations of the cation.[9] Figure 2a shows the calorimetric traces of the sample published previously.[9] No phase changes in the RTIL were observed on cooling from the liquid state above the melting point to 183 K. On heating, through the glass transition at 192 K it shows cold crystallization at 226.5 K. Then, [C_4mim]PF_6 experiences two

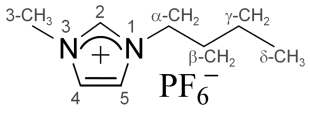

Figure 1. Structure of [C_4mim]PF_6 and numbering system.

Received: January 18, 2012
Revised: March 1, 2012
Published: March 1, 2012

ACS Publications © 2012 American Chemical Society

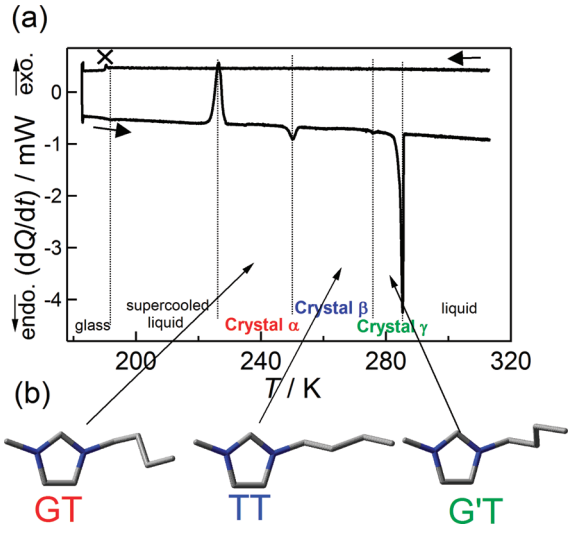

Figure 2. (a) Calorimetric traces of $[C_4mim]PF_6$.[9] "X" in the cooling represents an experimental artifact. (b) The cation conformations for each crystalline phase, i.e., GT, TT, G'T, reported in ref 9.

solid−solid phase changes at 250.3 and 276.1 K and melts at 285.3 K. The observed three crystalline phases are referred to crystals α, β, and γ in the order of increasing temperature. They have different butyl group conformations in the cation, i.e., gauche−trans (GT), trans−trans (TT), and gauche′−trans (G′T), as shown in Figure 2b. This result indicates that the variety of ion conformations plays an important role in the thermal phase behavior of imidazolium-based RTILs.

However, despite our Raman spectroscopic and calorimetric investigations,[9] the thermal phase behavior of $[C_4mim]PF_6$ is not yet completely understood. The complexity of the thermal phase behavior appears in the inconsistency between ion structures determined by X-ray crystal structure analyses[32,34] and Raman spectroscopy.[9] Single crystal X-ray diffraction clarified that the cation structure of $[C_4mim]PF_6$ forms the G′T conformation at 173 and 193 K,[32,34] whereas the Raman spectra indicated that the G′T conformation only exists in the temperature range of 276−285 K.[9] In addition, it is intriguing that the thermal phase changes accompanied with conformational changes, as observed in this PF_6 salt, have not yet been reported in other $[C_4mim]^+$-based RTILs, e.g., Cl,[35−38] Br,[35,37−39] I,[38,40] BF_4,[38] and $N(CF_3SO_2)_2$[41−44] salts. Therefore, the thermal phase behavior of $[C_4mim]PF_6$ is worth pursuing. Furthermore, note that the thermal phase behavior of $[C_4mim]PF_6$ has been recently investigated under high pressure.[45−49]

In this study, we investigated the cation dynamics of the representative RTIL $[C_4mim]PF_6$ in the crystalline states to understand its complex thermal phase behavior. Note that there are several papers reporting the ion dynamics of RTILs in the liquid state, but very few papers elucidate the same in the crystalline state. ^{1}H NMR spectroscopy was performed to estimate the spin−lattice and spin−spin relaxation times (T_1 and T_2, respectively) as well as the second moment of the spectra (M_2), which provide information on the rotational dynamics of the cation.

EXPERIMENTAL SECTION

$[C_4mim]PF_6$ was purchased from Kanto Chemical Co., Inc. The sample was washed with distilled water several times; the absence of halide ions was confirmed by the $AgNO_3$ test. The sample was dried at ca. 333 K for 1 day under 10^{-3} Pa before use and sealed in a 10-mm NMR tube in vacuum; this procedure reduces the water content of RTILs to less than 150 ppm.[38]

NMR measurements were performed using a Fourier transform pulse NMR instrument (MU25, JEOL, ^{1}H resonance frequency: 25 MHz). Temperature of the sample was controlled at cooling and heating rates of approximately 5−10 K/min. T_1 was measured with the inversion recovery method. T_2 was measured with the Carr−Purcell−Meiboom−Gill (CPMG) method[50,51] for the liquid phase above 243 K and the solid echo method[52] for other solid-like states. T_2 values were derived from the free induction decay (FID) signal using the following Weibull function:

$$M(t) = M_0 \exp\left(-\left(\frac{t}{T_2}\right)^n\right) \quad (1)$$

where $M(t)$ and M_0 are the sample magnetization at times t and $t = 0$, respectively, and n is the Weibull coefficient. The solid echo method was also applied to estimate M_2 of the ^{1}H NMR spectra. Propylammonium chloride, whose M_2 was previously determined,[53] was used to obtain the accurate parameter τ in the solid echo pulse sequence, $90_x-\tau-90_y$. The NMR instrument having a low magnetic field used in this study measures the averaged relaxation times and FID signals of ^{1}H nuclei in the sample. A nonlinear regression method (Levenberg−Marquardt) was used for theoretical fitting of the FID and T_1 data.

Density functional theory (DFT) calculations were performed using the Gaussian 03 program package.[54] Full geometry optimization analyses for the ions in the gas phase were performed using 6-311+G(d,p) basis sets on the basis of Becke's three-parameter hybrid method[55] with the LYP correlation (B3LYP).[56,57] The calculations in the gas phase are known to provide useful insights into the structure and dynamics of RTILs.[36,58−60] No imaginary frequencies were produced by the optimized structures; this ensured the presence of a minimum.

Raman spectra were measured by a Raman spectrometer (HoloLab 5000, Kaiser Optical Systems) combined with a lab-built calorimeter.[61] The spectrometer is fitted with an optical fiber and a GaAlAs diode laser (wavelength: 785 nm). A spectrum in the range of 100−3450 cm^{-1} can be measured at once with a resolution of 4 cm^{-1}. This system enables us to observe the heat flow in the sample with a temperature stability of ±0.001 K during Raman scattering experiments.

RESULTS AND DISCUSSION

A. T_1 and T_2 Plots. Figure 3a shows T_1 and T_2 plots of $[C_4mim]PF_6$ during cooling and heating. The plots change continuously with decreasing temperature to 173 K with cooling from the liquid state. On the other hand, sudden jumps on heating at 233, 253, and 283 K were observed. Above 283 K, these jumps are completely superimposed on the plots of the liquid state, which indicates that the third jump at 283 K is due to melting of the sample. Considering previous calorimetric results,[9] the first and second jumps originate from the cold crystallization of RTIL (i.e., the formation of crystal α) and the phase change from crystal α to β, respectively. In fact, the Raman spectrum of each state (data not shown) is in good agreement with the previous result.[9] Although crystal γ was not

dx.doi.org/10.1021/jp300636s | J. Phys. Chem. B 2012, 116, 3780−3788

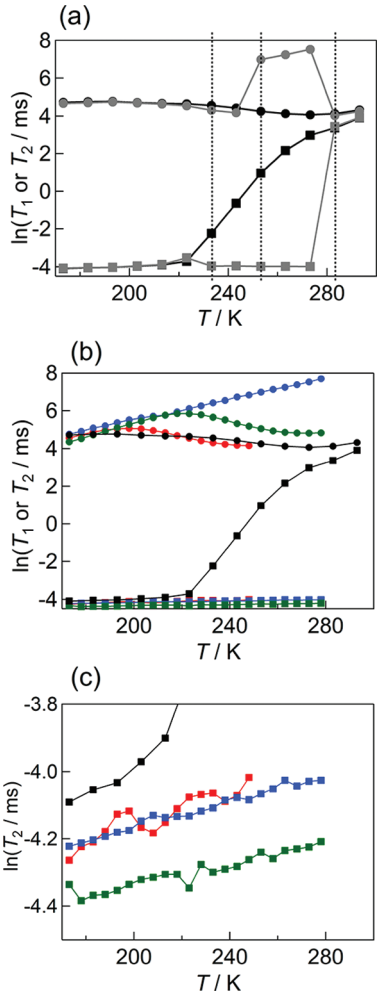

Figure 3. (a) T_1 (filled circles) and T_2 (filled squares) plots during cooling (black) and heating (gray). The dashed lines represent sudden jumps of T_1 and T_2 plots on heating. (b) Temperature dependence of T_1 and T_2. Red, blue, and green symbols are relaxation times for crystals α, β, and γ. Black ones are at liquid, supercooled liquid, or glassy states. (c) T_2 plot enlargement.

observed in the present thermal history, it was obtained from crystal β after cooling at 273 or 257 K for 1 day or 225 K for 1 week (crystal γ was also examined by Raman spectroscopy). The extremely slow phase change from crystal β to γ suggests that the activation energy of the phase change is considerably high. Such phase change would be affected by the heating rate and the amount of the sample which differ from the previous Raman experiments.[9] Note that ^{1}H T_1 and T_2 behaviors of $[C_4mim]PF_6$ are similar to those of $[C_4mim]Br$,[62,63] except the existence of the solid−solid phase changes.

When each crystalline phase was cooled to 173 K from below their phase change point, their T_1 and T_2 values varied continuously, as shown in Figure 3b. This suggests that the phase changes between the crystalline phases in the solid state are irreversible and are assigned to structural relaxation rather than phase transition ("structural relaxation" can occur at any temperatures while "phase transition" must occur at the phase transition temperature with the value of zero in the Gibbs free energy difference), as previously observed in 1,3-dimethylimidazolium hexafluorophosphate.[64] Note that the phase change from crystal β to γ occurs at various temperatures (i.e., structural relaxation); thus, crystal γ would be more stable than crystal β considering Gibbs free energy in the temperature range of 273−225 K.

T_1 and T_2 plots of each crystalline phase show different curves as a function of temperature. This suggests that each phase possesses different rotational dynamics of the cation. Figure 3c shows an enlargement of the T_2 plots. Here, because the inverse of T_2 positively correlates with the averaged correlation times of ^{1}H nuclei, it is suggested that the averaged mobility of the cation in each crystalline phase is in the order of $\gamma < \beta \leq \alpha$. Quantitative analyses using second moment calculations and T_1 curve fits are discussed in the following section.

B. M_2 Calculations for Motion Type Estimation.

1. Theoretical M_2. M_2 calculations of ^{1}H NMR spectra were performed to investigate the type of motion occurring in each crystalline state. In general, M_2 is the variance and is represented as

$$M_2 = \frac{\int(\omega - M_1)^2 f(\omega)\mathrm{d}\omega}{\int f(\omega)\mathrm{d}\omega} \tag{2}$$

where M_1 is the first moment. The theoretical M_2 values of ^{1}H NMR spectra, summarized in Table 1, are estimated by the following procedure. First, the theoretical rigid lattice M_2 was estimated using the Van Vleck equation,[65]

$$M_2 = \frac{3}{5}\gamma_H^2\hbar^2 N^{-1} I(I+1)\sum_{j,k} r_{jk}^{-6} + \frac{4}{15}\gamma_S^2\hbar^2 N^{-1} \times S(S+1)\sum_{j,f} r_{jf}^{-6} \tag{3}$$

where γ_H and γ_S is the gyromagnetic ratios of proton and heteronuclear, respectively, $\hbar$ is the reduced Planck's constant, N is the number of nuclei, I and S are the nuclear spin quantum numbers for the proton and heteronuclear spins, respectively, and r is the distance between spin pairs j and k or j and f. Because the solid echo method mainly refocuses the dipole−dipole coupling of homonuclear spins,[66] only H−H contributions were considered to calculate the theoretical M_2 value.

Table 1. Theoretical Second Moment (M_2) Values (in Gauss^2) for $[C_4mim]PF_6$ in the Crystalline States

	intracation	intercation <3.5 Å	intercation >3.5 Å	total
rigid lattice	17.7	2.6	1.7	22.0
3-CH_3 rotation	14.1	2.6	1.7	18.5
3-CH_3 + δ-CH_3 rotations	10.8	1.9	1.7	14.4
isotropic rotation of cation	0.0	0.0	1.7	1.7

The theoretical M_2 was estimated as the sum of intra- and intercation (≤3.5 Å and >3.5 Å) contributions. The intracation M_2 was calculated on the basis of the cation structure optimized by Gaussian 03 and giving very similar values for the GT, TT, and G′T conformations (17.7, 17.6, and 17.7 G^2, respectively). Therefore, the value 17.7 G^2 was used for all the crystals.

For M_2 from the intercation contributions, because of the lack of crystal structure data for α and β phases, the crystal structure of the γ phase with the G′T conformation of the cation[32] was applied to other crystals, which would be a reasonable assumption as explained in the following. Let us consider the intercation M_2 values of two analogue RTILs

dx.doi.org/10.1021/jp300636s | J. Phys. Chem. B 2012, 116, 3780−3788

1-butyl-3-methylimidazolium chloride ([C_4mim]Cl) and 1-butyl-2,3-dimethylimidazolium chloride ([C_4C_1mim]Cl). Similar to [C_4mim]PF_6, both RTILs were reported to exhibit crystal polymorphism and have two crystals with different cation conformations for the butyl group, i.e., TT and GT. The intercation M_2 values of the TT and GT conformations for [C_4mim]Cl are estimated to be 5.6 and 6.1 G^2, and those for [C_4C_1mim]Cl are 5.8 and 6.2 G^2, respectively, from each crystal structure.[35,67] The difference in the intercation M_2 between the polymorphic crystals of these RTILs is ca. 0.5 G^2. The difference is expected to be smaller in the [C_4mim]PF_6 crystals because the distance between the protons in different cations increases because the ion size of PF_6^- is larger than that of Cl^-. Therefore, the discrepancy of the intercation contributions due to different polymorphic crystals would not largely appear in the total M_2 values of the [C_4mim]PF_6 crystals.

When the distance between the protons in different cations is less than 3.5 Å, each intercation interaction was calculated. Because the M_2 value derived from the 3.5 Å H−H distance is calculated to be 0.026 G^2, it can be considered that the value is small enough to be neglected as an individual contribution. Then, the contributions from the H−H distance larger than 3.5 Å were estimated using the following equation[68] on the basis of the crystal structure[32]

$$M_2 = 358.1 \times 4\pi N_p (3M^3V)^{-1} \quad (4)$$

where N_p is the number of protons per unit cell, M is the cutoff radius (here 3.5 Å), and V is the unit cell volume. This equation assumes a continuous distribution of protons at a proton distance larger than 3.5 Å.

When rapid rotation of a certain group occurs, the M_2 value is reduced by a factor of[69]

$$\rho = \frac{1}{4}(3\cos^2\theta - 1)^2 \quad (5)$$

where θ is the angle between the interproton vector and the reorientation axis. Note that protons of a certain group in rapid rotation were assumed to be positioned in their center of gravity.[70] Considering that a certain rotational motion of [C_4mim]$^+$ in the crystalline states occurs, either of the two methyl groups at the 3 position of the imidazolium ring (3-CH_3) or the terminal of the butyl group (δ-CH_3) in the cation would be responsible for the fastest rotation. Figure 4

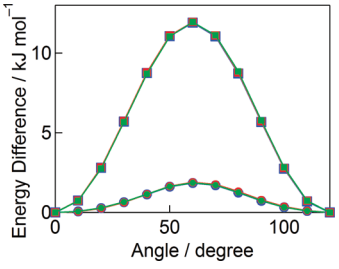

Figure 4. Potential energy surfaces for the two methyl group rotations. Filled circles: 3-CH_3; filled squares: δ-CH_3. Red: GT, blue: TT, green: G′T. The fact that the potential energy is almost independent of the cation conformation causes overlapping of the energy surfaces.

shows the calculated potential energy surfaces of the two methyl group rotations in [C_4mim]$^+$. Because the activation energies (E_a) of 3-CH_3 and δ-CH_3 rotations are calculated to be 1.9 and 11.9 kJ mol^{-1}, respectively, 3-CH_3 should rotate faster than δ-CH_3. In other words, 3-CH_3 rotation is considered to be the fastest rotational motion of the cation in the crystalline states. Note that because E_a hardly differs among GT, TT, and G′T conformers, all plots in Figure 4 overlap each other.

Finally, we obtain the M_2 value of 22.0 G^2 for the rigid lattice structure. When the 3-CH_3 rotation as the fastest motion in the cation occurs, M_2 is reduced to 18.5 G^2 by 3.5 G^2. The rotation of the additional methyl group (δ-CH_3) reduces M_2 to 14.4 G^2. If the rapid isotropic rotation of the cation exists in the crystal, M_2 is drastically reduced to 1.7 G^2 with no contributions from intra- and intercations having a proton distance less than 3.5 Å.

2. Observed M_2. The experimental M_2 values were estimated from the FID signals measured with the solid echo method using the following equations[71]

$$M(t) = M_0 \exp\left(-\frac{a^2}{2}t^2\right)\frac{\sin bt}{bt} + \text{baseline} \quad (6)$$

$$M_2 = \frac{1}{\gamma_H^2}\left(a^2 + \frac{1}{3}b^2\right) \quad (7)$$

All FID signals obtained here included a minor component introduced as *baseline* in eq 6, which is less than 10% in signal intensity compared to the major component. The minor component is considered to be an artifact, and it is assumed that the expression is the same as that of the first term of eq 6. The signals were well fitted with eq 6, as shown in Figure 5.

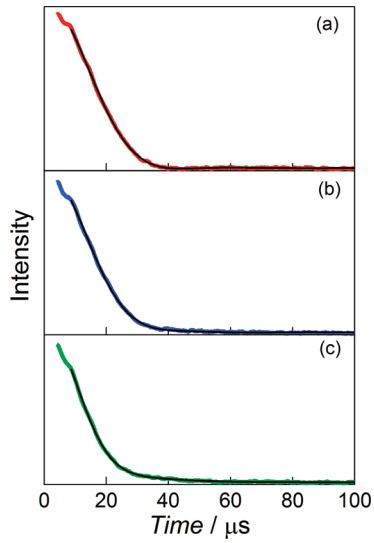

Figure 5. Theoretical fitting (black lines) to the FID signals at 233 K. (a) Crystal α (red), (b) crystal β (blue), and (c) crystal γ (green). The fitting was performed with a decay time from 8.6 to 100 μs.

Figure 6 shows the temperature dependence of the experimental M_2 values. The dashed line in the figure denotes the theoretical value when 3-CH_3 and δ-CH_3 rotations occur (14.4 G^2). The figure shows three important insights into the rotational dynamics of [C_4mim]PF_6 in the crystalline states. First, almost every plot is below the dashed line, which demonstrates that both methyl groups in [C_4mim]$^+$ rotate rapidly in the crystalline states. Second, the fact that all plots are below the line verifies the existence of certain rotational motions in addition to the two methyl group rotations. This is also confirmed by the fact that all M_2 curves decrease with increasing temperature. If no rotation occurred in addition to

dx.doi.org/10.1021/jp300636s | J. Phys. Chem. B 2012, 116, 3780−3788

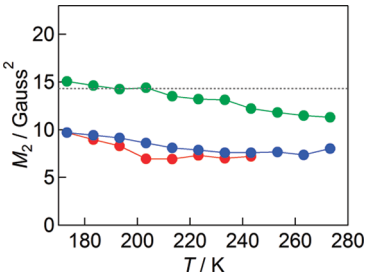

Figure 6. Temperature dependence of the second moment M_2 for crystal α (red), crystal β (blue), and crystal γ (green). The gray dashed line is the theoretical value when both 3-CH_3 and δ-CH_3 rotations occur (14.4 G^2).

the methyl group rotations in the crystalline states, the values should be constant, i.e., temperature independence. It is reasonable to argue that the additional motions are segmental motions of the butyl group in the cation because of its high flexibility compared to the imidazolium ring. The crystal structure data of some $[C_4mim]^+$-based RTILs demonstrate that the butyl group has a thermal vibration larger than that of the imidazolium ring.[32,35,40,72,73] It is considered that the segmental motions are not large-angle but small-angle rotation (or librational motion) because large-angle rotation is reminiscent of the conformational change of the butyl group, which would make the chain lose the conformational difference among the crystals. Finally, it can be deduced from the figure that the M_2 values follow the trend $\gamma > \beta \geq \alpha$, which indicates that the mobility of the segmental motions follows this trend in the reverse order. Note that the result of the observed M_2 is in good agreement with that of the T_2 value, as shown in Figure 3c.

3. Relationship between M_2 and Crystal Packing Density. The origin of the difference in the rotational mobility between the three crystals could be related to cation−anion interactions (or crystal packing). To estimate these interactions, Raman spectra in the high-frequency region were measured for the three crystals. The results are displayed in Figure 7 and summarized in Table 2. The Raman peaks in the range of 3140−3200 cm^{-1} include three vibrational modes, i.e., the stretching mode of the C−H bond at the 2 position of the imidazolium ring (C(2)−H) and the symmetric and asymmetric stretching modes of C−H bonds at the 4 and 5 positions (C(4)−H/C(5)−H). Although the Raman band assignments of imidazolium-based RTILs in this region are still debatable,[74−77] previous discussions have argued that all the three bands, i.e., C(2)−H[74,77−86] and symmetric[38,74,80,81,84,86−88] and asymmetric[80,86] C(4)−H/C(5)−H stretching modes, shift to lower frequency when the distance between the protons and the anions decreases. This is consistent with the harmonic oscillator model, i.e., when a stronger interaction exists between protons and anions, Raman peaks shift to lower frequency because of the decrease in the force constant of the C−H bonds. The calculated peak positions for these modes hardly change depending on the conformation of the cation. However, distinguishable peak shifts were observed in the experimental Raman peaks. The order of the lowering frequency shift for the average peak position is $\gamma > \beta > \alpha$. These findings reveal that the strength of the cation−anion interactions follows this trend. This result explains the order of the M_2 values: $\gamma > \beta \geq \alpha$. In other words, the small distance between the cation and the anion (or close packing) causes the restriction of the segmental motions of the butyl group, resulting in a larger M_2 value.

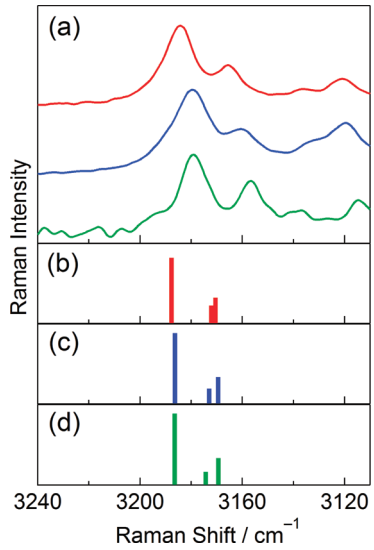

Figure 7. Raman spectra in the range of 3110−3240 cm^{-1}. (a) The experimental spectra for crystal α at 233 K (red), crystal β at 263 K (blue), and crystal γ at 277 K (green). The theoretical bands for (b) GT, (c) TT, and (d) G′T for free $[C_4mim]^+$ cation. The value of 0.9679 was used as the scaling factor for the theoretical Raman bands.[94]

Table 2. Observed and Theoretical Raman Stretching Bands in the High-Frequency Region (cm^{-1})[a]

	mode	crystal α	crystal β	crystal γ
observed	C(2)−H + C(4)−H/C(5)−H asymmetric	3166	3161	3157
	C(4)−H/C(5)−H symmetric	3184	3179	3179
theoretical	C(4)−H/C(5)−H asymmetric	3169.4	3169.5	3170.6
	C(2)−H	3174.4	3173.0	3172.1
	C(4)−H/C(5)−H symmetric	3186.5	3186.4	3187.7

[a]The value of 0.9679 was used as the scaling factor for the theoretical Raman bands.[94]

C. T_1 Curve Fits for Nanosecond Rotational Dynamics. The nanosecond rotational dynamics was estimated from ^1H T_1 analyses. There are five mechanisms for NMR relaxation, i.e., relaxation by magnetic dipole−dipole T_1^{DD}, chemical shift anisotropy T_1^{CSA}, spin rotation T_1^{SR}, scalar T_1^{Sc}, and quadrupole T_1^{Q} interactions. For proton-rich samples such as $[C_4mim]PF_6$, we can consider only T_1^{DD} contribution as the relaxation mechanism. Homonuclear T_1^{DD} is explained as[89]

$$\frac{1}{T_1^{DD}} = C[J(\omega_H) + 4J(2\omega_H)] \tag{8}$$

$$C = \frac{2}{3}\gamma_H^2 \Delta M_2 \tag{9}$$

$$J(\omega_H) = \frac{\tau_c}{1 + (\omega_H \tau_c)^2} \tag{10}$$

$$\tau_c = \tau_0 \exp\left(\frac{E_a}{RT}\right) \tag{11}$$

where C is the motional constant, ΔM_2 is a part of the second moment averaged by the considered motion, ω_j is the

dx.doi.org/10.1021/jp300636s | J. Phys. Chem. B 2012, 116, 3780−3788

frequency, $J(\omega)$ is the spectral density, τ_c is the rotational correlation time, τ_0 is the correlation time at infinite temperature, E_a is the activation energy, and R is the gas constant. The theoretical fitting was performed using these equations, as shown in Figure 8. The fitting reveals that there

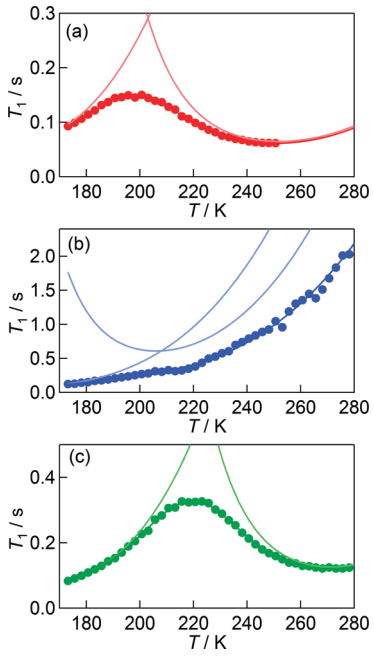

Figure 8. Theoretical fitting to the observed T_1 plots: (a) crystal α, (b) crystal β, and (c) crystal γ. The simulation of ^{1}H T_1 data is represented by the dark shade, and the individual simulation components for the low and high temperature dynamical components are indicated by the light shade.

are two components in the T_1 plots of all the crystals, which are referred to as the fast and slow rotational motions. Although one may see only one component in the T_1 plots of crystal β, two components are required to adequately fit the data because of the existence of the slight minimum around ca. 210 K. The parameters obtained from the T_1 fitting, ΔM_2, E_a, and τ_0, are summarized in Table 3.

Considering the methyl group rotation, C in eq 9 can be written as[90−92]

$$C = \frac{N_{\mathrm{methyl}}}{N_{\mathrm{all}}}\frac{9}{20}\frac{\gamma_{\mathrm{H}}^4\hbar^2}{r_{\mathrm{methyl}}^6} \qquad (12)$$

where N_{methyl} and N_{all} are the numbers of protons in the methyl group and the molecule, respectively, and r_{methyl} is the average distance between the protons in the methyl group. From eqs 9 and 12, the ΔM_2 values for 3-CH_3 and δ-CH_3 rotations are estimated to be 3.4 and 3.6 G^2, respectively. Theoretical M_2 analyses indicated that 3-CH_3 and δ-CH_3 rotations decreased in M_2 by 3.5 and 4.1 G^2, respectively (see Table 1). The fast rotational motion for the three crystals derived from the T_1 fittings is estimated to be ca. 3 G^2 in ΔM_2 and has E_a values similar to 12.5−15.1 kJ mol^{-1}. On the basis of these findings, the fast motion can be assigned to the rotation of either 3-CH_3 or δ-CH_3. The estimated E_a values were similar to the calculated E_a values for the δ-CH_3 rotation, i.e., 11.9 kJ mol^{-1}, as shown in Figure 4. Therefore, the fast motion observed in the T_1 plots of all three crystals is attributed to the δ-CH_3 rotation. This assignment is reasonable because the calculated E_a for the 3-CH_3 rotation is 1.9 kJ mol^{-1}, which is also in good agreement with the E_a of 1.28 kJ mol^{-1} estimated from the neutron scattering measurements.[30] A slight discrepancy in ΔM_2 was observed between experimental and calculated values as ca. 3 and 3.6 or 4.1 G^2, respectively. This would be due to the uncertainty of ΔM_2 in the T_1 measurements. The T_1 measurements did not appear to cover sufficient temperature range in order to estimate the fast motion with high accuracy because the minimum of the T_1 curve for the fast motion is not observed here (see Figure 8).

There is diversity of ΔM_2 and E_a for the slow motion among the three crystalline phases. The relatively large ΔM_2 values in crystals α and γ indicate that their slow motions would be a certain segmental motion of the butyl group, whose presence was demonstrated in the previous section. Their ΔM_2 values are distinguishable, which indicates that they have different segmental motions. The smaller ΔM_2 value in crystal γ (1.8 G^2) than in crystal α (3.6 G^2) indicates the slower or smaller segmental motion of the butyl group in crystal γ. This is consistent with the result of observed M_2 shown in Figure 6. The ΔM_2 value in crystal β (0.4 G^2) is small to be considered as the segmental motion. It might be related to a certain PF_6^- rotational motion because the ΔM_2 value is comparable to that of the PF_6^- isotropic rotation (0.5 G^2). It should be noted that the values 0.4 G^2 and 0.5 G^2 are not adequate to be compared because the former is obtained as the homonuclear contribution (see eqs 8 and 9) and the latter, which is calculated using the second term of eq 3, is obtained as the heteronuclear one. The small segmental motion of the butyl group or a certain rotational motion of the anion would be regarded as the slow motion in crystal β.

Rotational correlation times τ_c were derived from the ^{1}H T_1 fitting. Figure 9a and 9b shows the temperature dependence of τ_c for the fast (i.e., δ-CH_3 rotation) and slow rotational motions, respectively. The τ_c values for the slow motions are ca. 10^2 larger than that for the δ-CH_3 rotations. Conspicuous diversity in τ_c values was observed in the slow motions of the three crystalline phases, whereas τ_c for δ-CH_3 rotations slightly

Table 3. Parameters Derived from T_1 Measurements[a]

	crystal α		crystal β		crystal γ	
	fast	slow	fast	slow	fast	slow
ΔM_2 (Gauss^2)	3.3	3.6	2.8	0.4	2.8	1.8
E_a (kJ mol^{-1})	12.5 ± 1.4	20.1 ± 1.0	14.6 ± 10.9	16.7 ± 9.7	15.1 ± 0.4	26.8 ± 0.6
τ_0 (fs)	269	260	51	235	73	27

[a]A part of the second moment averaged by the considered motion ΔM_2, rotational activation energy E_a, rotational correlation time at infinite temperature τ_0 for the fast and slow motions. E_a values are shown with standard deviation (SD) determined by the fitting of T_1 plots which represents the experimental error. Closer location of T_1 minimum of the two components in crystal β make the fitting more difficult, which results in SD values larger than the others.

dx.doi.org/10.1021/jp300636s | J. Phys. Chem. B 2012, 116, 3780−3788

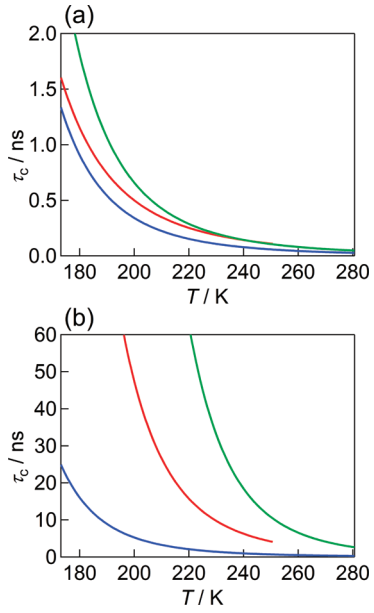

Figure 9. Rotational correlation times τ_c derived from T_1 fitting for (a) the fast rotational motion that is assigned to δ-CH_3 rotation and for (b) the slow rotational motion. Red: crystal α, blue: crystal β, and green: crystal γ.

depends on the crystalline phase. The diversity arises from the different types of slow motion. The orders of the correlation time for the fast and slow motions are $\gamma > \alpha > \beta$. Both trends are not consistent with that of closer packing estimated by high-frequency Raman spectra. It is suggested that the nanosecond rotational motions observed here would be governed by local interactions; hence, they do not appear to be significantly affected by crystal packing density. In addition, the mobility of the segmental motions is likely to change significantly with the conformation of the butyl group.

CONCLUSION

The existence of three crystals, α, β, and γ, in the representative RTIL $[C_4mim]PF_6$ was confirmed by ^1H NMR relaxation measurements, and it is supported by our previous Raman spectroscopic and calorimetric measurements. The phase changes between the crystals did not occur during cooling, which suggests that they are irreversible and likely to be structural relaxations rather than phase transitions.

M_2 analyses revealed that the segmental motions of the butyl group in addition to 3-CH_3 and δ-CH_3 rotations occurred in all the crystals. The experimental M_2 values are in the order of $\gamma > \beta \geq \alpha$, which indicates that γ has the slowest segmental motions. Raman spectra measurements in the high-frequency region indicate that γ has the strongest cation−anion interactions (or closest packing), leading to the slowest segmental motions.

Two nanosecond rotational motions were observed for all the phases from the T_1 results. The fast motion was assigned to the δ-CH_3 rotation, and E_a was determined to be 12.5−15.1 kJ mol^{-1}, which is similar to 11.9 kJ mol^{-1} estimated by quantum chemical calculations of the cation in the gas phase. The difference between the observed and calculated E_a suggests that δ-CH_3 and probably 3-CH_3 in the crystalline phases experience rotational barriers slightly higher than those in the gas phase. 3-CH_3 rotations would be considerably fast to be observed by the present NMR instrument because they have very small E_a (1−2 kJ mol^{-1}). The slow rotational motion observed in the T_1 results could originate from the segmental motion of the butyl group for α and γ, and the small segmental motion or a certain PF_6^- rotational motion for crystal β. Although the mobility of the fast and slow motions changes with the crystalline states, the trends of the correlation times are not consistent with crystal packing density. This is because such nanosecond rotational motions would be affected by local interactions rather than packing density, and particularly with respect to the segmental motions, the mobility is likely to change significantly with the conformation of the butyl group.

Crystal γ can be regarded as the most stable phase because of the slowest segmental motion and the strongest cation−anion interactions. In summary, our results explain why crystal γ was observed at 173 and 193 K in the previous single-crystal structure analyses although it appears to contradict our Raman spectroscopy and calorimetry results.

AUTHOR INFORMATION

Corresponding Author

*Fax: +81-43-290-3939. E-mail: k.nishikawa@faculty.chiba-u.jp.

Notes

The authors declare no competing financial interest.

ACKNOWLEDGMENTS

The present study was supported by the Ministry of Education, Culture, Sports, Science and Technology of Japan No. 21245003 Grant-in-Aid for Scientific Research (A) and the Global Center-of-Excellence Program "Advanced School for Organic Electronics".

REFERENCES

(1) *Ionic Liquids in Synthesis*; Wasserscheid, P., Welton, T., Eds.; VCH-Wiley: Weinheim, Germany, 2003.
(2) *Electrochemical Aspects of Ionic Liquids*; Ohno, H., Ed.; Wiley-Interscience: Hoboken, 2005.
(3) Welton, T. *Chem. Rev.* **1999**, *99*, 2071−2083.
(4) Wasserscheid, P.; Keim, W. *Angew. Chem., Int. Ed.* **2000**, *39*, 3772−3789.
(5) Sheldon, R. *Chem. Commun.* **2001**, 2399−2407.
(6) Kabo, G. J.; Blokhin, A. V.; Paulechka, Y. U.; Kabo, A. G.; Shymanovich, M. P.; Magee, J. W. *J. Chem. Eng. Data* **2004**, *49*, 453−461.
(7) Jin, H.; O'Hare, B.; Dong, J.; Arzhantsev, S.; Baker, G. A.; Wishart, J. F.; Benesi, A. J.; Maroncelli, M. *J. Phys. Chem. B* **2008**, *112*, 81−92.
(8) Troncoso, J.; Cerdeiriña, C. A.; Sanmamed, Y. A.; Romaní, L.; Rebelo, L. P. N *J. Chem. Eng. Data* **2006**, *51*, 1856−1859.
(9) Endo, T.; Kato, T.; Tozaki, K.; Nishikawa, K. *J. Phys. Chem. B* **2010**, *114*, 407−411.
(10) Tomida, D.; Kumagai, A.; Qiao, K.; Yokoyama, C. *Int. J. Thermophys.* **2006**, *27*, 39−47.
(11) Branco, L. C.; Rosa, J. N.; Moura Ramos, J. J.; Afonso, C. A. M. *Chem.—Eur. J.* **2002**, *8*, 3671−3677.
(12) Jacquemin, J.; Husson, P.; Padua, A. A. H.; Majer, V. *Green Chem.* **2006**, *8*, 172−180.
(13) Harris, K. R.; Woolf, L. A.; Kanakubo, M. *J. Chem. Eng. Data* **2005**, *50*, 1777−1782.
(14) Tokuda, H.; Tsuzuki, S.; Susan, M. A. B. H.; Hayamizu, K.; Watanabe, M. *J. Phys. Chem. B* **2006**, *110*, 19593−19600.
(15) Pereiro, A. B.; Legido, J. L.; Rodríguez, A. *J. Chem. Thermodyn.* **2007**, *39*, 1168−1175.
(16) Morrow, T. I.; Maginn, E. J. *J. Phys. Chem. B* **2002**, *106*, 12807−12813.

(17) Antony, J. H.; Mertens, D.; Breitenstein, T.; Dölle, A.; Wasserscheid, P.; Carper, W. R. *Pure Appl. Chem.* **2004**, *76*, 255−261.
(18) Urahata, S. M.; Ribeiro, M. C. C. *J. Chem. Phys.* **2005**, *122*, 024511.
(19) Shah, J. K.; Brennecke, J. F.; Maginn, E. J. *Green Chem.* **2002**, *4*, 112−118.
(20) Liu, Z.; Huang, S.; Wang, W. *J. Phys. Chem. B* **2004**, *108*, 12978−12989.
(21) Schröder, C.; Rudas, T.; Steinhauser, O. *J. Chem. Phys.* **2006**, *125*, 244506.
(22) Karimi-Varzaneh, H. A.; Müller-Plathe, F.; Balasubramanian, S.; Carbone, P. *Phys. Chem. Chem. Phys.* **2010**, *12*, 4714−4724.
(23) Roy, D.; Patel, N.; Conte, S.; Maroncelli, M. *J. Phys. Chem. B* **2010**, *114*, 8410−8424.
(24) Hardacre, C.; Holbrey, J. D.; Mullan, C. L.; Youngs, T. G. A.; Bowron, D. T. *J. Chem. Phys.* **2010**, *133*, 074510.
(25) MacChiagodena, M.; Gontrani, L.; Ramondo, F.; Triolo, A.; Caminiti, R. *J. Chem. Phys.* **2011**, *134*, 114521.
(26) Tsuzuki, S.; Shinoda, W.; Saito, H.; Mikami, M.; Tokuda, H.; Watanabe, M. *J. Phys. Chem. B* **2009**, *113*, 10641−10649.
(27) Tokuda, H.; Hayamizu, K.; Ishii, K.; Susan, M. A. B. H.; Watanabe, M. *J. Phys. Chem. B* **2004**, *108*, 16593−16600.
(28) Shirota, H.; Nishikawa, K.; Ishida, T. *J. Phys. Chem. B* **2009**, *113*, 9831−9839.
(29) Nakamura, K.; Shikata, T. *ChemPhysChem* **2010**, *11*, 285−294.
(30) Triolo, A.; Russina, O.; Hardacre, C.; Nieuwenhuyzen, M.; Gonzalez, M. A.; Grimm, H. *J. Phys. Chem. B* **2005**, *109*, 22061−22066.
(31) Rivera, A.; Brodin, A.; Pugachev, A.; Rössler, E. A. *J. Chem. Phys.* **2007**, *126*, 114503.
(32) Choudhury, A. R.; Winterton, N.; Steiner, A.; Cooper, A. I.; Johnson, K. A. *J. Am. Chem. Soc.* **2005**, *127*, 16792−16793.
(33) Triolo, A.; Mandanici, A.; Russina, O.; Rodriguez-Mora, V.; Cutroni, M.; Hardacre, C.; Nieuwenhuyzen, M.; Bleif, H.-J.; Keller, L.; Ramos, M. A. *J. Phys. Chem. B* **2006**, *110*, 21357−21364.
(34) Dibrov, S. M.; Kochi, J. K. *Acta Crystallogr., Sect. C: Cryst. Struct. Commun.* **2006**, *C62*, o19−o21.
(35) Holbrey, J. D.; Reichert, W. M.; Nieuwenhuyzen, M.; Johnston, S.; Seddon, K. R.; Rogers, R. D. *Chem. Commun.* **2003**, 1636−1637.
(36) Hayashi, S.; Ozawa, R.; Hamaguchi, H. *Chem. Lett.* **2003**, *32*, 498−499.
(37) Nishikawa, K.; Wang, S.; Katayanagi, H.; Hayashi, S.; Hamaguchi, H.; Koga, Y.; Tozaki, K. *J. Phys. Chem. B* **2007**, *111*, 4894−4900.
(38) Endo, T.; Kato, T.; Nishikawa, K. *J. Phys. Chem. B* **2010**, *114*, 9201−9208.
(39) Ozawa, R.; Hayashi, S.; Saha, S.; Kobayashi, A.; Hamaguchi, H. *Chem. Lett.* **2003**, *32*, 948−949.
(40) Nakakoshi, M.; Shiro, M.; Fujimoto, T.; Machinami, T.; Seki, H.; Tashiro, M.; Nishikawa, K. *Chem. Lett.* **2006**, *35*, 1400−1401.
(41) Blokhin, A. V.; Paulechka, Y. U.; Kabo, G. J. *Thermochim. Acta* **2006**, *445*, 75−77.
(42) Blokhin, A. V.; Paulechka, Y. U.; Strechan, A. A.; Kabo, G. J. *J. Phys. Chem. B* **2008**, *112*, 4357−4364.
(43) MacFarlane, D. R.; Meakin, P.; Amini, N.; Forsyth, M. *J. Phys.: Condens. Matter* **2001**, *13*, 8257−8267.
(44) Fredlake, C. P.; Crosthwaite, J. M.; Hert, D. G.; Aki, S. N. V. K.; Brennecke, J. F. *J. Chem. Eng. Data* **2004**, *49*, 954−964.
(45) De Azevedo, R. G.; Esperança, J. M. S. S.; Najdanovic-Visak, V.; Visak, Z. P.; Guedes, H. J. R.; Ponte, M. N. D.; Rebelo, L. P. N *J. Chem. Eng. Data* **2005**, *50*, 997−1008.
(46) Su, L.; Li, L.; Hu, Y.; Yuan, C.; Shao, C.; Hong, S. *J. Chem. Phys.* **2009**, *130*, 184503.
(47) Su, L.; Li, M.; Zhu, X.; Wang, Z.; Chen, Z.; Li, F.; Zhou, Q.; Hong, S. *J. Phys. Chem. B* **2010**, *114*, 5061−5065.
(48) Takekiyo, T.; Hatano, N.; Imai, Y.; Abe, H.; Yoshimura, Y. *High Pressure Res.* **2011**, *31*, 35−38.
(49) Russina, O.; Fazio, B.; Schmidt, C.; Triolo, A. *Phys. Chem. Chem. Phys.* **2011**, *13*, 12067−12074.
(50) Carr, H. Y.; Purcell, E. M. *Phys. Rev.* **1954**, *94*, 630−638.
(51) Meiboom, S.; Gill, D. *Rev. Sci. Instrum.* **1958**, *29*, 688−691.
(52) Powles, J. G.; Strange, J. H. *Proc. Phys. Soc.* **1963**, *82*, 6−15.
(53) Albert, S.; Ripmeester, J. A. *J. Chem. Phys.* **1978**, *69*, 3967−3971.
(54) Frisch, M. J.; Trucks, G. W.; Schlegel, H. B.; Scuseria, G. E.; Robb, M. A.; Cheeseman, J. R.; Montgomery, J. A., Jr.; Vreven, T.; Kudin, K. N.; Burant, J. C.et al. *Gaussian 03*; Gaussian, Inc., Wallingford, CT, 2004.
(55) Becke, A. D. *J. Chem. Phys.* **1993**, *98*, 5648−5652.
(56) Lee, C.; Yang, W.; Parr, R. G. *Phys. Rev. B* **1988**, *37*, 785−789.
(57) Miehlich, B.; Savin, A.; Stoll, H.; Preuss, H. *Chem. Phys. Lett.* **1989**, *157*, 200−206.
(58) Umebayashi, Y.; Fujimori, T.; Sukizaki, T.; Asada, M.; Fujii, K.; Kanzaki, R.; Ishiguro, S. *J. Phys. Chem. A* **2005**, *109*, 8976−8982.
(59) Hunt, P. A. *J. Phys. Chem. B* **2007**, *111*, 4844−4853.
(60) Tsuzuki, S.; Arai, A. A.; Nishikawa, K. *J. Phys. Chem. B* **2008**, *112*, 7739−7747.
(61) Endo, T.; Tozaki, K.; Masaki, T.; Nishikawa, K. *Jpn. J. Appl. Phys.* **2008**, *47*, 1775−1779.
(62) Imanari, M.; Nakakoshi, M.; Seki, H.; Nishikawa, K. *Chem. Phys. Lett.* **2008**, *459*, 89−93.
(63) Imanari, M.; Uchida, K.; Miyano, K.; Seki, H.; Nishikawa, K. *Phys. Chem. Chem. Phys.* **2010**, *12*, 2959−2967.
(64) Endo, T.; Morita, T.; Nishikawa, K. *Chem. Phys. Lett.* **2011**, *517*, 162−165.
(65) Van Vleck, J. H. *Phys. Rev.* **1948**, *74*, 1168−1183.
(66) Powles, J. G.; Mansfield, P. *Phys. Lett.* **1962**, *2*, 58−59.
(67) Andre, M.; Loidl, J.; Laus, G.; Schottenberger, H.; Bentivoglio, G.; Wurst, K.; Ongania, K. H. *Anal. Chem.* **2005**, *77*, 702−705.
(68) Ibers, J. A.; Stevenson, D. P. *J. Chem. Phys.* **1958**, *28*, 929−938.
(69) Gutowsky, H. S.; Pake, G. E. *J. Chem. Phys.* **1950**, *18*, 162−170.
(70) Andrew, E. R.; Eades, R. G. *Proc. R. Soc. London, Ser. A* **1953**, *216*, 398−412.
(71) *Principles of Nuclear Magnetism*; Abragam, A., Ed.; Oxford University Press: Oxford, 1961.
(72) Paulechka, Y. U.; Kabo, G. J.; Blokhin, A. V.; Shaplov, A. S.; Lozinskaya, E. I.; Golovanov, D. G.; Lyssenko, K. A.; Korlyukov, A. A.; Vygodskii, Y. S. *J. Phys. Chem. B* **2009**, *113*, 9538−9546.
(73) Santos, C. S.; Rivera-R., S.; Dibrov, S.; Baldelli, S. *J. Phys. Chem. C* **2007**, *111*, 7682−7691.
(74) Köddermann, T.; Wertz, C.; Heintz, A.; Ludwig, R. *ChemPhysChem* **2006**, *7*, 1944−1949.
(75) Lassègues, J. C.; Grondin, J.; Cavagnat, D.; Johansson, P. *J. Phys. Chem. A* **2009**, *113*, 6419−6421.
(76) Wulf, A.; Fumino, K.; Ludwig, R. *J. Phys. Chem. A* **2010**, *114*, 685−686.
(77) Grondin, J.; Lassègues, J.-C.; Cavagnat, D.; Buffeteau, T.; Johansson, P.; Holomb, R. *J. Raman Spectrosc.* **2011**, *42*, 733−743.
(78) Katsyuba, S. A.; Dyson, P. J.; Vandyukova, E. E.; Chernova, A. V.; Vidiš, A. *Helv. Chim. Acta* **2004**, *87*, 2556−2565.
(79) Xuan, X.; Guo, M.; Pei, Y.; Zheng, Y. *Spectrochim. Acta, Part A* **2011**, *78*, 1492−1499.
(80) Chang, H. C.; Jiang, J. C.; Tsai, W. C.; Chen, G. C.; Lin, S. H. *J. Phys. Chem. B* **2006**, *110*, 3302−3307.
(81) Katsyuba, S. A.; Zvereva, E. E.; Vidiš, A.; Dyson, P. J. *J. Phys. Chem. A* **2007**, *111*, 352−370.
(82) Holomb, R.; Martinelli, A.; Albinsson, I.; Lassègues, J. C.; Johansson, P.; Jacobsson, P. *J. Raman Spectrosc.* **2008**, *39*, 793−805.
(83) Chang, H. C.; Jiang, J. C.; Su, J. C.; Chang, C. Y.; Lin, S. H. *J. Phys. Chem. A* **2007**, *111*, 9201−9206.
(84) Berg, R. W.; Deetlefs, M.; Seddon, K. R.; Shim, I.; Thompson, J. M. *J. Phys. Chem. B* **2005**, *109*, 19018−19025.
(85) Gao, Y.; Zhang, L.; Wang, Y.; Li, H. *J. Phys. Chem. B* **2010**, *114*, 2828−2833.
(86) Jeon, Y.; Sung, J.; Seo, C.; Lim, H.; Cheong, H.; Kang, M.; Moon, B.; Ouchi, Y.; Kim, D. *J. Phys. Chem. B* **2008**, *112*, 4735−4740.
(87) Noack, K.; Schulz, P. S.; Paape, N.; Kiefer, J.; Wasserscheid, P.; Leipertz, A. *Phys. Chem. Chem. Phys.* **2010**, *12*, 14153−14161.

(88) Fumino, K.; Wulf, A.; Ludwig, R. *Angew. Chem., Int. Ed.* **2008**, *47*, 8731−8734.
(89) Bloembergen, N.; Purcell, E. M.; Pound, R. V. *Phys. Rev.* **1948**, *73*, 679−712.
(90) Yukitoshi, T.; Suga, H.; Seki, S.; Itoh, J. *J. Phys. Soc. Jpn.* **1957**, *12*, 506−515.
(91) Stejskal, E. O.; Gutowsky, H. S. *J. Chem. Phys.* **1958**, *28*, 388−396.
(92) O'Reilly, D. E.; Tsang, T. *Phys. Rev.* **1967**, *157*, 417−426.
(93) Reichert, W. M.; Holbrey, J. D.; Swatloski, R. P.; Gutowski, K. E.; Visser, A. E.; Nieuwenhuyzen, M.; Seddon, K. R.; Rogers, R. D. *Cryst. Growth Des.* **2007**, *7*, 1106−1114.
(94) Andersson, M. P.; Uvdal, P. *J. Phys. Chem. A* **2005**, *109*, 2937−2941.